Gyroscopic Stabilization of a Kid-Size Bicycle

Pom Yuan Lam

Nanyang Polytechnic
180 Ang Mo Kio Ave 8 Singapore 569830
POM_Yuan_Lam@nyp.gov.sg

***Abstract*—This paper reports the design and development of a self-balancing bicycle using off the shelf electronics. A self-balancing bicycle is a non-linear unstable system similar to that of an inverted pendulum. Experimental results show the robustness and efficiency of a proportional plus derivative (PD) controller balancing the bicycle. The system uses a control moment gyroscope (CMG) as an actuator for balancing.**

***Keywords*— Bicycle, Control Moment Gyro (CMG), Real-Time, Control and FPGA.**

I. INTRODUCTION

The bicycle is a good mean of transportation because of its advantages of environmental friendliness and light weight. A bicycle robot is naturally an unstable nonlinear system. Its inherent nonlinearity makes the problem of controlling it difficult and, as a result, brings interesting challenges to the control engineering community. Researchers have been exploring different mechatronic solutions to dynamically balance and manoeuvre bicycle robots.

A self-balancing bicycle robot is a bicycle equipped with sensors to detect the roll angle of the bicycle and actuators to bring it back to the balancing position whenever it deflects from it, similar to an inverted pendulum. It is a nonlinear unstable system.

There are several methods by which a self-balancing bicycle robot can be implemented. In this report, we introduce these methods, and focus on one of the mechanisms which involve the use of a Control Moment Gyro (CMG), an attitude control device typically used in spacecraft attitude control systems [1]. A CMG consists of a spinning rotor and one or more motorized gimbals that tilt the rotor's angular momentum. As the rotor tilts, the changing angular momentum causes a gyroscopic precessive torque that balances the bicycle.

II. REVIEW OF PREVIOUS WORK

A bicycle is inherently unstable and without proper control, it is uncontrollable and cannot be balanced. There are several different methods used for balancing of bicycle robots, such as the use of gyroscopic stabilisation by Beznos et al. in 1998 [2], Gallaspy in 1999 [3], moving of the centre of gravity or mass balancing by Lee and Ham in 2002 [4], and steering control by Tanaka and Murakami in 2004 [5]. A very well-known self-balancing bicycle robot is the Murata Boy which was developed by Murata in 2005. Murata Boy (Fig. 1) makes use a Reaction Wheel as an actuator to balance the bicycle. It uses a reaction wheel which is mounted in the robot's body as a torque generator to balance itself. A reaction wheel consists of a spinning rotor, whose spin rate is nominally zero. Its spin axis is fixed to the bicycle, and its speed is increased or decreased to generate reaction torque about the spin axis. Reaction wheel are the simplest and least expensive of all momentum-exchange actuators. Advantage of such system is that is low cost, simple and no ground reaction. The disadvantage is that it consumes more energy and it is not capable of producing large amounts of torque.

In another approach proposed by Gallaspy [3], the bicycle can be balanced by controlling the torque exerted on the steering handle bar. Based on the amount of roll a controller will control the amount of torque applied to the steering handle bar to balance the bicycle. Advantage of such system is low mass and low energy consumption. Its disadvantage is that it requires ground reaction forces and such system will not be able to withstand large roll disturbance.

Among these methods, CMG also known as gyroscopic stabilizer is a good choice as the response time is short and the system can be stable even when the bicycle is stationary. Control Moment Gyro (CMG) consists of a spinning rotor with large, constant angular momentum, but whose angular momentum vector direction can be changed with respect to bicycle by rotating the spinning rotor. The spinning rotor is mounted on a gimbal, and applying torque to the gimbal results in a precessional, gyroscopic reaction torque orthogonal to both the rotor spin and gimbal axes. The CMG is a torque amplification device because small gimbal torque input produces large control torque on the bicycle. The robot described in this paper uses a CMG as a momentum exchange actuator to balance the bicycle. Advantage of such system is that it is capable of producing large amount of torque and has no ground reaction forces. Disadvantage is that such system consumes more energy and is heavier.

Fig. 1. Murata Boy, self-balancing bicycle riding robot.

978-1-61284-200-4/11/$26.00 ©

III. DYNAMIC MODEL OF CMG-CONTROLLED BICYCLE

The bicycle relies on the gyroscopic precessive torque to stabilise the bicycle in an upright position. Fig. 2 shows how the precession torque balances the bicycle.

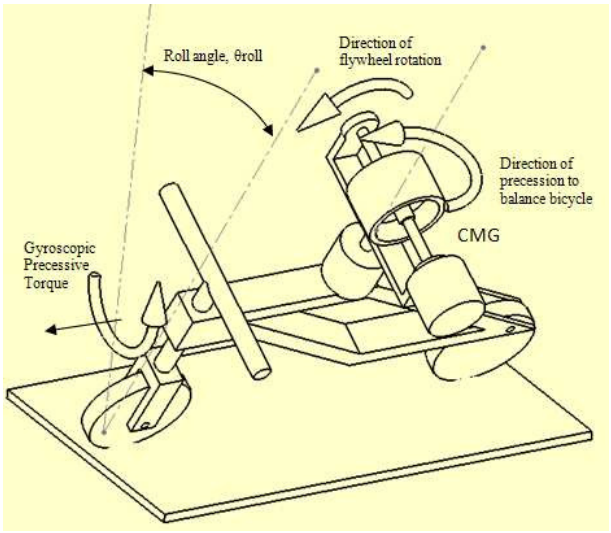

Fig. 2. Balancing of bicycle using gyroscopic precessive torque generated by CMG.

When the bicycle is tilted at an angle θ_{roll} as shown in Fig. 2, an IMU sensor would detect the roll angle. This roll data is feed to an onboard controller which in turn will command the CMG's gimbal motor to rotate such that a gyroscopic precessive torque is produced to balance the bicycle to an upright position.

The system uses a single gimbal CMG and generated only one axis torque and direction of output torque change is in accordance with gimbal motion. Fig. 3 shows the various components and vectors of a single gimbal CMG. The system makes use of the gyroscopic torque to balance the bicycle.

The flywheel angular nominal speed is 4480 rpm hence; ω_{fly} is 469 rad/s.

Angular momentum of rotor, $Z = J\omega_{fly}$
$= 0.00883 \times 469$
$= 4.14$ kg-m^2/s

If a rotational precessive rate of W_D, is applied to the spinning flywheel about the gimbal axis, a precessive output torque, T, which is perpendicular to the direction of ω_{fly} and ω_D will be generated as shown in Fig. 3. Gimbal motor is capable of an angular velocity of 5 rad/s, the gimbal precessive output torque, generated is therefore

$$T_p = Z\omega_D$$
$$= 4.14 \times 5$$
$$= 20.7 \text{ Nm}$$

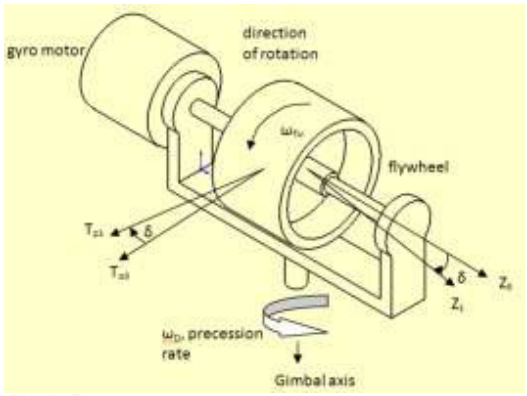

Definition
$\omega_{flywheel}$ is flywheel angular velocity
Z_0 is flywheel angular momentum vector at time t
Z_1 is flywheel angular momentum vector at time (t + dt)
δ is precession angular displacement
Tp_0 is the precessive output torque at time t
Tp_1 is the precessive output torque at time (t + dt)

Material of flywheel	Brass
Mass	2.02kg
Polar moment of inertia, J	8.83E-3 kgm^2
Radius of gyration, k	0.066m
Diameter	0.153m
Power	12 W

Fig. 3. Various component of a single axis CMG.

The dynamic model of a bicycle is based on equilibrium of gravity and centrifugal forces. A simplified model for balancing purpose is derived using Lagrange method by neglecting forces generated from moving forward and steering of the bicycle. This model is based on the work of Parnichkun[2]. With reference to Fig. 4, the system made up of two rigid body links, first link is the bicycle frame that has one degree-of-freedom (DOF) rotation about the Z axis. Second link is the flywheel. The flywheel is assumed to have constant speed ω. Centre of gravity of flywheel is fixed relative to the bicycle frame.

When the flywheel rotates with a constant speed about X1-axis and we control angular position of the gimbal axis around Y1-axis, angular momentum on Z1-axis will generate a torque. This torque is called precession torque generated by gyroscopic effect, and will be used to balance the bicycle.

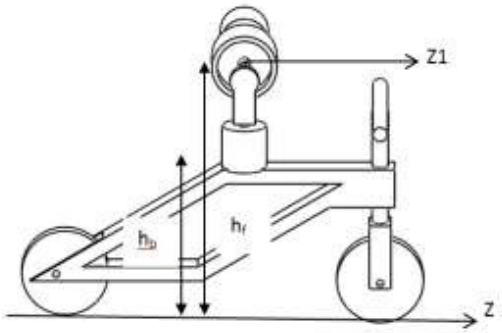

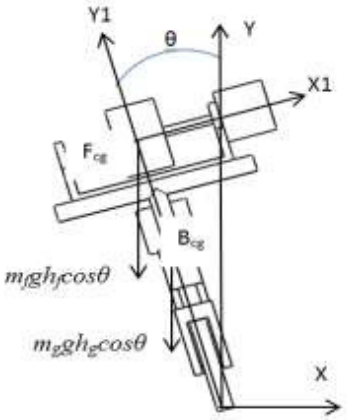

Fig. 4. Reference coordinates of bicycle.

In Fig. 4, B_{cg} and F_{cg} denotes bicycle and flywheel centres of gravity, respectively. The roll angle about Z-axis is defined by θ, and angular position of the gimbal axis of flywheel around Y1-axis as shown in Fig. 4. The angular velocity of the bicycle around Z axis is defined as $\dot{\theta}$, and the angular velocity of the flywheel around its gimbal axis is defined as $\dot{\delta}$. Since flywheel centre of gravity does not move related to the bicycle centre of gravity, absolute velocities of B_{cg} and F_{cg} are:

$$|V_b| = \dot{\theta} h_B \quad (1)$$

$$|V_f| = \dot{\theta} h_f \quad (2)$$

where h_b is the height of the bicycle centre of gravity to ground and h_f is the height of the centre of gravity of flywheel to ground. Lagrange equation [6] is used to derive the dynamic model of the system,

$$\frac{d}{dt}\left\{\frac{\partial T}{\partial q_i}\right\} - \frac{\partial T}{\partial q_i} + \frac{\partial V}{\partial q_i} = Q_i \quad (3)$$

where T is the system total kinetic energy, V is system total potential, Qi is external forces, and qi is generalized coordinate. V and T are determined, and represented as follows.

$$V = m_b g h_b \cos\theta + m_f g h_f \cos\theta \quad (4)$$

$$T = \frac{1}{2} m_b (|v_b|)^2 + \frac{1}{2} m_f \left(|v_f|\right)^2 + \frac{1}{2} I_b \dot{\theta}^2 + \frac{1}{2}\left[I_r \dot{\delta}^2 + I_p \left(\dot{\theta} \sin\delta\right)^2 + I_r \left(\dot{\theta} \cos\delta\right)^2\right]$$

$$T = \frac{1}{2} m_b \left(\dot{\theta}^2 {h_b}^2\right) + \frac{1}{2} m_f \left(\dot{\theta}^2 {h_f}^2\right) + \frac{1}{2} I_b \dot{\theta}^2 + \frac{1}{2}\left[I_r \dot{\delta}^2 + I_p \left(\dot{\theta} \sin\delta\right)^2 + I_r \left(\dot{\theta} \cos\delta\right)^2\right] \quad (5)$$

where I_p is the flywheel polar moment of inertia and I_r is flywheel radial moment of inertia, m_b is mass of bicycle and m_f is the mass of flywheel mass. I_b is bicycle moment of inertia.

For $q_i = \theta$, the Lagrange equation becomes

$$\frac{d}{dt}\left\{\frac{\partial T}{\partial \dot{\theta}}\right\} - \frac{\partial T}{\partial \theta} + \frac{\partial V}{\partial \theta} = Q_\theta \quad (6)$$

Using Equations (4)-(6), we have

$$\ddot{\theta}[m_b h_b^2 + m_f h_f^2 + I_b + I_p sin^2\delta + I_r cos^2\delta] + 2 sin\delta cos\delta \left(I_p - I_r\right)\dot{\theta}\dot{\delta} - g\left(m_b h_b + m_f h_f\right) sin\theta = I_p \omega \dot{\delta} cos\delta \quad (7)$$

For $q_i = \delta$, the Lagrange equation becomes

$$\frac{d}{dt}\left\{\frac{\partial T}{\partial \dot{\delta}}\right\} - \frac{\partial T}{\partial \delta} + \frac{\partial V}{\partial \delta} = Q_\delta \quad (8)$$

Using Equations (4), (5) and (8), the following equation is derived.

$$\ddot{\delta} I_r - \dot{\theta}^2 \left(I_p - I_r\right) sin\delta cos\delta = T_m - I_p \omega \dot{\theta} cos\delta - B_m \dot{\delta} \quad (9)$$

where B_m is DC motor viscosity coefficient. The DC motor is coupled to the gimbal of the Flywheel via a final 65:1 ratio of a combinational of planetary gearhead and belt-drive.

$$T_m = 65 K_m i \quad (10)$$

$$U = L\frac{di}{dt} + R_i + K_e \dot{\delta} \quad (11)$$

where K_m, K_e are torque and back emf constants of the motor, respectively. R and L are resistance and inductance of the motor, respectively. T_m is the torque generated by the motor and U is the voltage applied to the motor.

IV. SELF-BALANCING OF THE BICYCLE

Equations (7) – (9) shows the model of the dynamics of the bicycle. Equations (10) to (11) relates the torque generated with the voltage applied to the motor and represents the dynamics of the Electrical System.

Combining the equations result in

$$\ddot{\delta} I_r - I_p \omega \dot{\theta} + B_m \dot{\delta} - 65 K_m i = 0 \quad (12)$$

Linearization of the above equations about the equilibrium ($\theta = \delta = 0$) yields

$$\ddot{\theta}\left[m_b h_b^2 + m_f h_f^2 + I_b + I_r\right] - g\left(m_b h_b + m_f h_f\right)\theta - I_p \omega \dot{\delta} = 0 \quad (13)$$

Define $= \begin{bmatrix} \theta \\ \dot{\theta} \\ \delta \\ \dot{\delta} \end{bmatrix}$, $y = \theta$ and $u = U$. The dynamics model of the system in state-space representation by combining (11), (12) and (13) is shown by the following equation.

$$\dot{x} = Ax + Bu$$
$$y = Cx + Du \quad (14)$$

Where

$$A = \begin{bmatrix} 0 & 1 & 0 & 0 \\ \frac{g(m_b h_b + m_f h_f)}{m_b h_b^2 + m_f h_f^2 + I_b + I_r} & 0 & \frac{I_p \omega}{m_b h_b^2 + m_f h_f^2 + I_b + I_r} & 0 \\ 0 & -\frac{I_p \omega}{I_r} & -\frac{B_m}{I_r} & \frac{65 K_m}{I_r} \\ 0 & 0 & -\frac{K_e}{L} & -\frac{R}{L} \end{bmatrix}$$

$$B = \begin{bmatrix} 0 \\ 0 \\ 0 \\ \frac{1}{L} \end{bmatrix}, \quad C = [1 \quad 0 \quad 0 \quad 0], \text{ and } D = [0]. \quad (15)$$

Table 1 list the various parameters of the self-balancing robot.

Parameters	Value	Unit	Description
m_f	2.02	kg	Mass of flywheel
m_b	20.6	kg	Mass of bicycle
h_f	0.58	m	Flywheel c.g. upright height
h_b	0.49	m	Bicycle c.g. upright height
I_b	2.1	kg.m^2	Bicycle moment of inertia about ground contact line
I_p	0.0088	kg.m^2	Flywheel polar moment of inertia about c.g
I_r	0.0224	kg.m^2	Flywheel radial moment of inertia about c.g.
ω	469	rad/s	Flywheel angular velocity
L	0.000119	H	Motor Inductance
R	0.61	Ω	Motor Resistance
B_m	0.003	kg.m^2/s	Motor viscosity coefficient
K_m	0.0259	Nm/A	Motor torque constant
K_e	0.0027	V.s	Motor back emf constant
g	9.81	m/s^2	Gravitational acceleration

Table 1: Parameters of self-balancing robot.

Using the parameters from Table 1, the system matrices becomes

$$A = \begin{bmatrix} 0 & 1 & 0 & 0 \\ 14.14 & 0 & 0.972 & 0 \\ 0 & -184.6 & -0.133 & 75 \\ 0 & 0 & -22.69 & -5126 \end{bmatrix}$$

$$B = \begin{bmatrix} 0 \\ 0 \\ 0 \\ 8403 \end{bmatrix}, \quad C = [1 \quad 0 \quad 0 \quad 0], \text{ and } D = [0]. \quad (16)$$

Computing the transfer function from the state variables realization $(\boldsymbol{A}, \boldsymbol{B}, \boldsymbol{C}, \boldsymbol{D})$ yields

$$\frac{\theta(s)}{U(s)} = \frac{334019}{s^4 + 5126.16s^3 + 2470.7s^2 + 428419s - 34040} \quad (17)$$

Computer simulation is performed to assess the behaviour of the system. The software platform used was National Instruments Control Design Assistant.

A Pole-Zero Analysis was performed and it was found that there are four Poles and no Zero on the uncompensated system. Fig. 5 shows the Pole and Zero location for the uncompensated system and the system is unstable.

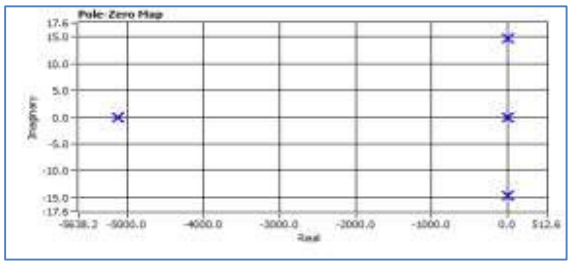

Fig. 5. Pole-Zero map of uncompensated system.

Fig. 6 shows the Bode Plot of the uncompensated system. The Gain Margin was -3.09 and Phase Margin was -44.04.

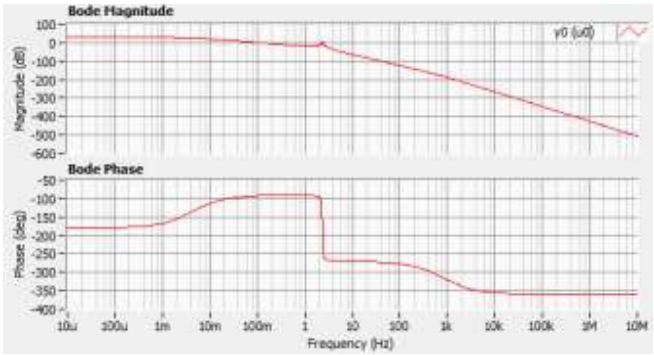

Fig. 6. Bode Plot of uncompensated system.

An internal loop Proportional plus Derivative controller was implemented in Control Design Assistant as shown in Fig. 7. The gains were selected by trial-and-error method P-Gain was selected to be 25 and D-gain was selected to be 0.02.

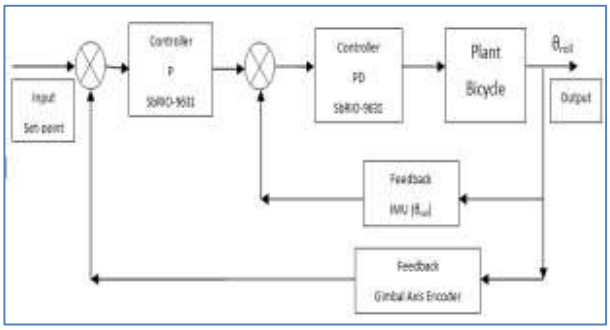

Fig. 7: Control block diagram.

Fig. 8 shows the Pole and Zero location for the compensated system and the system is stable.

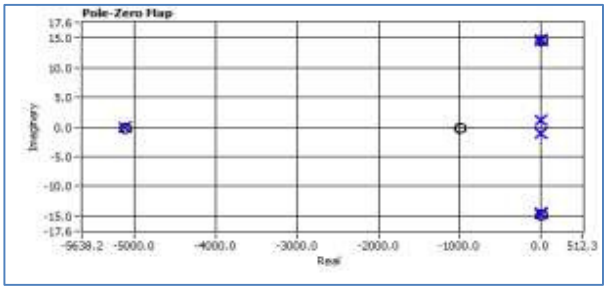

Fig. 8: Pole-Zero map of compensated system.

Fig. 9 shows the Bode Plot of the compensated system. The Gain Margin had improved to 6.59 and Phase Margin was 86.88. The compensated system is stable and poles and zeros cancellation can clearly be seen in Fig. 8. Fig. 10, shows the effect of increasing P-Gain. As can be seen from Fig. 10, overshoot increases with P-Gain.

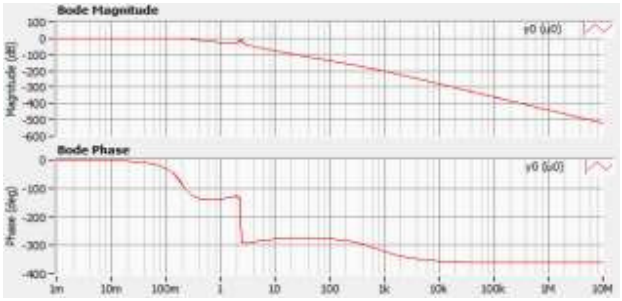

Fig. 9: Bode Plot of the compensated system.

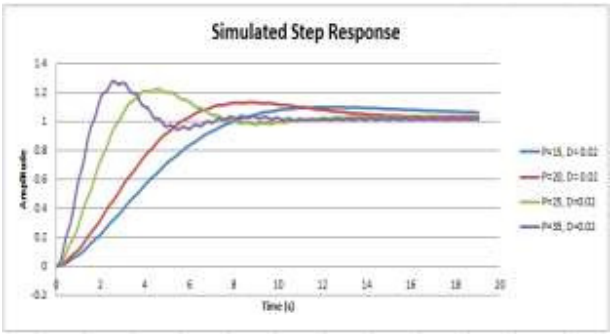

Fig. 10: Bode Plot of the compensated system.

Lastly, a PID controller was implemented instead of a PD controller. Fig. 11 shows the Pole-Zero map with a PID controller. The phase margin decreased drastically and the system will become unstable and unable to balance the bicycle.

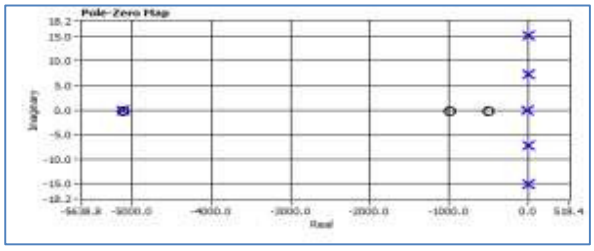

Fig. 11: Pole-Zero map of system with PID controller.

V. Real Time Experiments

Fig. 12 shows the complete mechanical system which consist of an off the shelf kid size bicycle and a custom made CMG mounted on the frame of the bicycle.


Fig. 12: Bicycle with CMG.

The embedded controller is the Single Board Reconfigurable IO (SbRIO) from National Instruments and Fig. 13 shows the internal block diagram of the SbRIO which consist of Freescale Power PC and Xilinx Spartan FPGA.

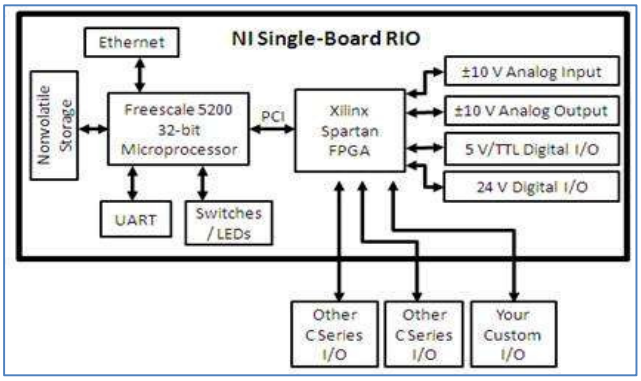

Fig. 13: Block Diagram of SbRIO.

An xsens MTi IMU is used to detect the roll angle of the bicycle. The MTi is a miniature, gyro-enhanced Attitude and Heading Reference System (AHRS). Its internal low-power signal processor provides drift-free 3D orientation as well as calibrated 3D acceleration, 3D rate of turn and 3D earth-magnetic field data. The MTi is an excellent measurement unit (IMU) for stabilization and control of cameras, robots, vehicles and other unmanned equipment. The MTi IMU communicates with the SbRIO via RS232 serial communication at a baud-rate of 115200bps.

The CMG's flywheel is driven by a Maxon DC motor and is powered by a constant dc voltage. The CMG gimbal is driven by another Maxon brushless motor and encoder signal are fed back to the FPGA of the SbRIO to be processed as angular positioning data.

In order to have a robust sensing system, differential encoder signal are fed back to the FPGA for processing and normally requires additional circuit such as an inverter and an OR gate as show in Fig. 14.

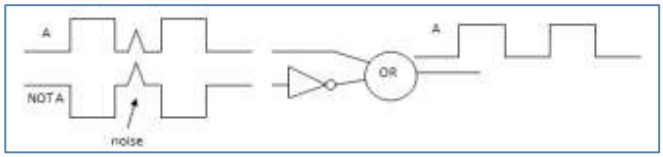

Fig. 14: Circuit to eliminate distortion by complementary encoder signals (differential).

With LabVIEW for FPGA, this can be easily implemented within the FPGA without the need for physical additional circuit. Finally, a pc connected via the Ethernet to the SbRIO for software development and tuning of gains. Fig. 15 summarises the complete electronic system.

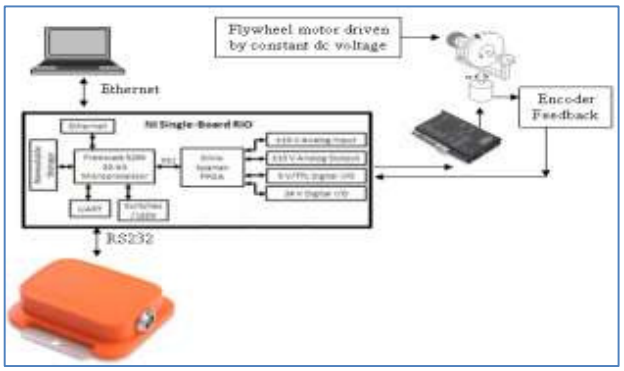

Fig. 15: Various sub component of the electronic system.

Critical encoder positioning data are being sampled by the FPGA and analog output voltage to control gimbal motor is sent from FPGA. The closed loop PID controller resides in the Freescale Power PC real time processor. With LabVIEW Real-Time, tuning of PID gains were done on the fly via Ethernet connection.

Experiment was conducted to determine the response of the system to a step input. Fig. 16 shows the setup of the test. The bike is initially tilted at an angle of 11.6 deg and the controller commands the bicycle to an upright position. The final gains used for the inner PD loop was Proportional Gain of 35 and Derivative Gain of 0.002, while the Proportional Gain for the outer loop was 0.17. Fig. 17 shows the response of the system with the gains.

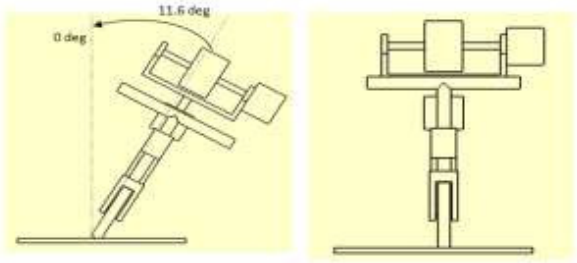

Fig. 16: Experiment setup for step response.

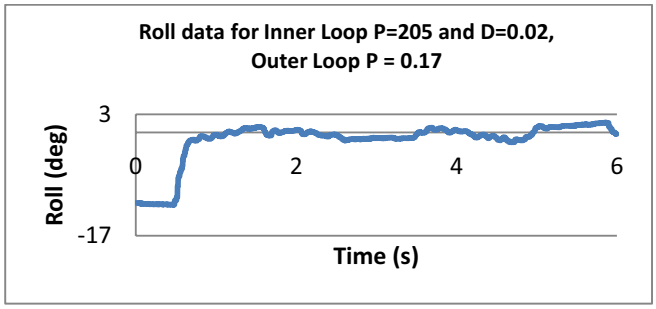

Fig. 17: Roll data.

The final gains selection is a tradeoff between performance and stability. As can be seen from Fig. 17, these gain sets produce a relativity fast response and acceptable steady state oscillation.

VI. Conclusions

This paper proposed the use of Control Moment Gyro (CMG) and a PD controller to balance a bicycle. CMG had been successfully used as a momentum exchange actuator to balance the bicycle. CMG is an effective actuator as it is a torque amplification device and has short response time.

A state space model of the bicycle with CMG and a closed loop controller had been created in Control Assistant; a product developed by National Instruments. Simulation were carried out to determine the performance of the controller and to find an initial gains to be used in a real time system for deployment. Through the various simulation exercises carried out, it can be deduced that a PD controller would be adequate to balance the bicycle. A PID controller would decrease the phase margin drastically and the system will become unstable and unable to balance the bicycle.

The real-time controller was implemented onto a SbRIO and was programmed in LabVIEW. This approach has drastically shortened the development time to achieve the PD controller, and is possible due to the easy of graphical LabVIEW programming, data could be easily view and manipulated at run-time.

References

[1] BUI, T.T. and Parnichkun, M. Balancing of Bicyrobo by particle swarm optimisation based structure-specified mixed H2/H∞ control. International Journal of Advanced Robotic Systems, 2008, **5**(4), 395-402.

[2] Beznos AV, Formalsky AM, Gurfinkel EV, Jicharev DN, Lensky AV, Savitsky K V, et al. Control of autonomous motion of two-wheel bicycle with gyroscopic stabilization. In:Proceedings of the IEEE international conference on robotics and automation, 1998, p. 2670-5.

[3] Gallaspy JM. Gyroscopic stabilization of an unmanned bicycle, M.S. Thesis, Auburn University, 1999.

[4] Lee S, Ham W. Self-stabilizing strategy in tracking control of unmanned electric bicycle with mass balance. IEEE international conference on intelligent robots and systems, 2002, p. 2200-5.

[5] Tanaka Y, Murakami T. Self sustaining bicycle robot with steering controller. In: Proceedings of international workshop on advanced motion control, 2004, p. 193-7.

[6] Wolfram S. Analytical robotics and mechatronics. New York: McGraw-Hill, 1995.